XL CILAMCE
IBERO-LATIN AMERICAN CONGRESS ON COMPUTATIONAL METHODS IN ENGINEERING
NOVEMBER 11-14, 2019
Praiamar Natal Hotel & Convention Natal, RN-BRAZIL

EXPERIMENTAL AND NUMERICAL STUDY OF MASONRY WITH EMPHASIS ON THE ANALYSIS OF STRUCTURAL EFFICIENCY

Anne C. L. Monteiro
anneclmonteiro@usp.br
Dept. of Structural Engineering, São Carlos School of Engineering, University of São Paulo
Av. Trabalhador São Carlense - 400, 13566-590, São Carlos/São Paulo, Brazil
Kildenberg K. F. Nunes
Hidelbrando J. F. Diógenes
Andrea B. Silva
Lays R. A. Costa
kildenberg@gmail.com.com
hidelbrando@ct.ufpb.br
andreabrasiliano@gmail.com
laysraianne@ct.ufpb.br
Dept. of civil and environmental engineering, Federal University of Paraíba
Cidade Universitária, 58051-900, João Pessoa/ Paraíba, Brazil

Abstract. In view of the speed and ease of execution, structures such as structural masonry are widely adopted in civil construction. Although this construction method is considered simple, for the elaboration of structural projects with satisfactory levels of security and economy, a comprehensive analysis of the structural behavior is essential. In this regard, numerical modeling is an efficient approach. In this work, it is carried out the numerical and experimental analysis of the mechanical performance of small walls of structural masonry, subjected to axial compression. To study the transmission mechanisms of the stresses and modes of failure, a linear analysis was performed from a homogenized model, developed in SAP2000® software. As a secondary aim, the strength of the masonry is compared to that of Light Steel Frame (LSF) panels constructed and modeled with geometric characteristics similar to those of the small masonry wall and their structural efficiencies was evaluated comparatively. From the obtained results, it was verified that the macromodeling is an efficient tool in the prediction of the strength transmission mechanisms in the masonry. About the investigation of the structural efficiency of the analyzed construction methods, a ratio of 2:1 was verified between the specific strength of the LSF and the structural masonry.

Keywords: Masonry, Axial compression, Macromodeling, Structural efficiency, Light Steel Frame.

1 Introduction

Structural masonry is a simple building system in which ceramic or concrete blocks and mortar joints are alternately arranged to form self-supporting structural walls. Due to the simplicity of construction process and low cost, self-supporting structures such as structural masonry are widely adopted in civil construction.

For the elaboration of structural projects with satisfactory levels of security and economy a comprehensive analysis of the structural behavior is essential. In this sense, numerical modeling is an efficient approach. Due to the heterogeneity, anisotropy and nonlinear behavior of the structural analysis the development of simple and representative numerical models is particularly complex., which has motivated the investigation of the subject by several researchers.

Numerical analysis of masonry can be developed by two different approaches: micro or macromodeling. In the first approach, discretization is performed at the level of the individual components, so mortar and block joints constitute independent parts in the model. In the second one, the block-mortar assembly is idealized as a homogeneous medium with equivalent properties. Although less refined and apparently less accurate, recent research has demonstrated the efficiency of macromodels in the analysis of global masonry strengths, providing both quality of the response and low computational cost (PELETEIRO [1]; LOURENÇO et. al [2]; TALIERCIO [3]; CASAPULLA [4]; NINO e LUONGO [5]).

The macromodeling proposes that a global constitutive law be defined based on the microconstitutive law and the block and mortar geometry. This law will relate the stresses and the average strains of a homogenized elementary set. In the linear elasticity analysis, several researchers have endeavored to propose analytical expressions that translate to equivalent properties of the macromodel.

The first contributions were made by Salamon [6] who analytically demonstrated that a heterogeneous and highly stratified material can be analyzed as a homogeneous and transversely isotropic continuous material. In their well-known study, the five elastic modules of the equivalent material were defined in terms of the properties and thickness of each layer. Pande et al. [7], exploring the results obtained by Salamon [6], proposed a two-stage homogenization technique (vertical and horizontal) widely used in the numerical analysis of structural masonry.

According to Nino and Luongo [5], although masonry exhibits nonlinear behavior, the evaluation of the global properties of the homogenized material in the elastic field is a relevant topic, since the research area has practical interest, since the technical norms still provide guidelines. The evaluation of the elastic properties of masonry and the formulas for the equivalent elastic material are implemented in various commercial software with recognized reliability.

In fact, elastic macromodeling is a structural analysis methodology with relevant practical interest for structural masonry design, which has motivated the continuous development of research. Nonetheless, a minority of the studies carried out to date confront theoretical predictions with experimental results. While numerical tools are versatile and analytical solutions refined, for reliable and representative response patterns, it is important that real models are evaluated and theoretical and experimental solutions compared.

This work presents a numerical and experimental study on the structural behavior of small structural masonry subject to axial compression. To study the mechanisms of fails and load transmission, a linear analysis had been carried through considering the linear elastic regimen and the technique of the homogenization approach in SAP2000® software. The results were validated with the experimental data.

As a secondary aim, the strength of the masonry is compared to that of Light Steel Frame (LSF) panels constructed and modeled with geometric characteristics similar to those of the small masonry wall (NUNES et al. [8]) and their structural efficiencies was evaluated comparatively.

2 Materials and methods

According to Barreto [9], numerical models can be used to analyze the load transfer mechanisms of a structural masonry panel and to satisfactorily evaluate the safety performance of the structure, provided that physical and mechanical parameters of the material have been obtained from laboratory tests. The quality of the response depends on the level of knowledge of material properties.

Thus, the numerical analysis performed in this study was preceded by an experimental program, from which the characterization tests of the materials used in the manufacture of small walls and axial compression tests of every small wall were performed.

2.1 Specimens description

Blocks (14×19×39 cm) and half blocks (14×19×19 cm) (Fig. 1.b) of concrete were used to construct six masonry walls with nominal dimensions of 120×120×14 (cm) (Fig. 1.a). The blocks were connected by vertical and horizontal mortar joints with an average size of 1 cm and in the laying of the blocks the mortar was distributed in both the longitudinal and vertical septa of the blocks (Fig. 1.c).

(a)

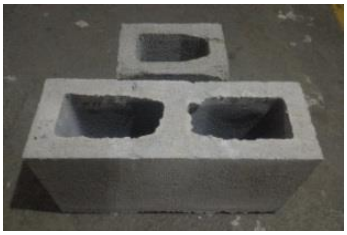

(b)

(c)

Figure 1. Experimental program: (a) mansory wall sample; (b) blocks and half blocks; (c) mortar joints

2.2 Physical and mechanical characterization tests

The experimental tests for physical and mechanical characterization of concrete blocks were carried out in accordance with the requirements of ABNT/NBR 12118 [10] and ABNT/NBR 6136 [11] standards and aimed to determine the properties of materials required for calibration of the numerical model.

To determine the effective dimensions of the blocks and half concrete blocks, measurements were made at three different points of the sample with a 0.01 mm precision caliper. The gross cross-sectional area (product between average width and length) and the net area, defined as the ratio between the volume of liquid displaced by a saturated block and the block height, according to the procedure recommended by ABNT/NBR 12118 [10] were also determined.

From the mechanical characterization tests were determined the axial compressive strength of the blocks (Fig. 2.a), prisms (Fig. 2.b) and mortar (Fig. 2.c), according to the technical standards ABNT/ NBR12118 [10], ABNT/NBR 16522[12] and ABNT/NBR 13279 [13], respectively.

(a) (b) (c)

Figure 2. Mechanical characterization tests of: (a) blocks (b) prisms; (c) mortars

Table 1 summarizes the physical and mechanical proprieties of blocks, half blocks, mortar and prisms obtained experimentally, in terms of mean, standard deviation and coefficient of variation.

Table 1 - Summary of material characterization test results (mean ± standard deviation [coefficient of variation - %])

Property	Block	Half block	Mortar	Prism
Length (cm)	39.14 ± 0.04 [0.11]	19.12 ± 0.02 [1.05]	-	-
Width (cm)	14.06 ± 0.05 [0.39]	14.06 ± 0.05 [0.36]	-	-
Height (cm)	19.4 ± 0.14 [0.73]	18.98 ± 0.13 [0.66]	-	-
Gross area (cm²)	550.44 ± 2.28 [0.41]	268.83 ± 2.09 [1.09]	-	-
Net area (cm²)	303.32 ± 5.79 [1.91]	165.75 ± 0.56 [0.34]	-	-
Net area/Gross area	0.55 ± 0.01 [1.91]	0.62 ± 0.002 [0.34]	-	-
Compressive strength (MPa)	2.94 ± 0.66 [22.40]	4.4 ± 0.71 [16.03]	11.32 ± 0.89 [7.90]	3.09 0.39 12.66]

2.3 Axial compression tests of small masonry walls

To analyze the structural performance, identifying failure modes and obtaining resistance and rigidity of masonry walls, axial compression tests were carried out in accordance with the Brazilian standard ABNT/NBR 16522 [12]. Fig. 3 presents the test setup.

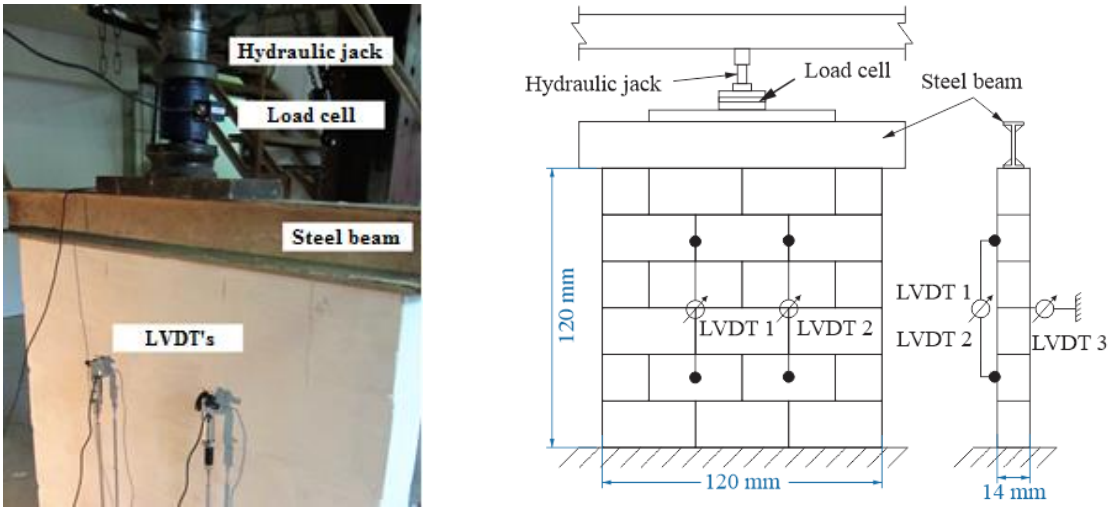

(a) (b)

Figure 3. Setup for axial compression tests in small masonry wall

To measure the displacements in the load direction, two LVDT (linear variable differential transformer) displacement transducers were used. On the opposite side a third LVDT was used to check for any horizontal displacements. The monotonic loading was applied with force control until the rupture of the small walls.

2.4 General aspects of numerical modeling via MEF

Determination of masonry macromodel elastic properties

Salamon [6] proposes a series of formulations (Eq. 1 a 6) to describe the behavior of the block-mortar assembly, considering the transverse isotropy of mechanical properties. The x, y and z axes conform to the global axes shown in Figure 4.

- Poisson's ratio in x and z directions

$$\upsilon'_1 = \frac{\sum_{i=1}^{2n} \frac{\phi_i \upsilon_{1i} E_{1i}}{1-\upsilon^2_{1i}}}{\sum_{i=1}^{2n} \frac{\phi_i E_{1i}}{1-\upsilon^2_{1i}}} \tag{1}$$

- Poisson's ratio in y direction

$$\upsilon'_2 = (1-\upsilon'_1)\sum_{i=1}^{2n} \frac{\phi_i \upsilon_{1i}}{1-\upsilon_{1i}} \tag{2}$$

- Modulus of elasticity in x and z directions

$$E'_1 = (1-\upsilon'^2_1)\sum_{i=1}^{2n} \frac{\phi_i E_{1i}}{1-\upsilon^2_{1i}} \tag{3}$$

- Modulus of elasticity in y directions

$$E'_2 = \frac{1}{\sum_{i=1}^{2n} \frac{\phi_i}{E_{1i}}\left[\frac{E_{1i}}{E_{2i}} - \frac{2\upsilon^2_{2i}}{1-\upsilon_{1i}}\right] + \frac{2\upsilon'^2_2}{(1-\upsilon'_1)E'_1}} \tag{4}$$

And each equation term means,

n: number of mortar block sets;
i 1,2,3...*n*;
ϕ_{2i-1}: relative height of the blocks given by:

$$\phi_{2(i-1)} = \frac{t_1}{\sum_{i=1}^{2n} t_i} \tag{5}$$

ϕ_{2i}: relative joint height given by:

$$\phi_{2i} = \frac{t_2}{\sum_{i=1}^{2n} t_i} \tag{6}$$

t: height, em cm;
υ: poisson's ratio;
E: modulus of elasticity tf/m².

In the above expressions the terms $(2i-1)$ e $(2i)$ refer to the properties of blocks and joints, respectively, and subscripts 1 and 2 to the x and z (plane) and y (transverse) directions, respectively.

The input data (block and mortar properties) required to obtain the physical properties of the homogenized material through the previous equations are presented in Table 2.

Table 2. Data used to obtain mechanical properties of homogenized material

Data	Unit	Value
Number of mortar block sets	und.	5
Block Height	cm	19
Mortar Height (Thickness)	cm	1
Poisson's ratio of blocks[1]	adm	0,2
Poisson's ratio of joints[2]	adm	0,2
Block modulus of elasticity	MPa	2815,17
Mortar modulus of elasticity	MPa	9053,33

[1] ABNT/NBR 15961-1 [14]; [2] ABNT/NBR 15630 [15].

The modulus of elasticity of the blocks (E_b) was calculated according to the procedure recommended by the ACI - Building Code 318 [16] (Eq. 7), as a function of the average block resistance (f_b) (Table 1) and the specific mass of the block. $(w_b = 1137\ kg/m^3)$, obtained experimentally.

$$\mathrm{E_b} = 0{,}0428\mathrm{f_b^{0,5}w_b^{1,5}} \tag{7}$$

Mortar modulus of elasticity (E_a) was estimated from the average compressive strength of mortar (f_{arg}) (Table 1) using Equation 8. The value of the constant α was assumed to be 800, an intermediate value between those recommended in the literature (SANTOS [17]).

$$\mathrm{E_a} = \alpha \mathrm{f_{arg}} \tag{7}$$

The average compressive strength of the mortar was obtained experimentally (Table 1). Although this value exceeds 70% of the block resistance in relation to the net area - which is in disagreement with the recommendation of ABNT/NBR 15961-1 [14]- it was purposely adopted, so that the ruin would occur with the block yield and not of the joint.

Table 3 presents the results obtained for the mechanical properties of the transverse isotropic homogenized material from the Salamon [6] equations. In Table 3, the compressive strength of the small masonry wall was calculated from the compressive strength of the prism (Table 1), according to the procedure of the standard ABNT/NBR 15961-1 [14].

Table 3 - Mechanical properties of transverse isotropic homogenized material obtained by Salamon [6]

Properties	Unit	Value
Poisson's ratio in x and z directions	adm	0,2
Poisson's ratio in the y direction	adm	0,2
Modulus of elasticity in x and z directions	MPa	3127,1
Y-modulus of elasticity	MPa	1591,2
Shear modulus in x and z directions	MPa	1303,0
Y-direction shear modulus	MPa	663,0
Wall density	kg/m³	1335,4
Compressive strength	MPa	2,54

Description of the analyzed numerical models

Numerical analysis in this work was performed based on macromodeling. This approach is simples and consists in model the masonry like a homogenized material, according to the procedure illustrated in Fig. 4.a. To compare the experimental stress-strain curves with numerical linear static analysis results, a homogenized macromodel was developed through SAP2000® (Fig. 4.b).

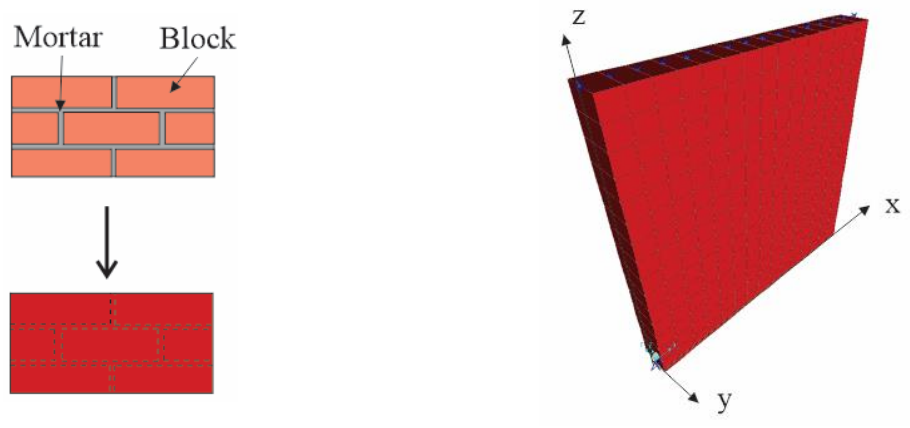

(a) (b)

Figure 4. (a) Homogenization technique; (b) Masonry macromodel on SAP2000®

The macromodel was simulated with a shell element with physical and mechanical properties (Table 3) of the homogenized model obtained by Salamon [6] expressions. In order to simulate of the actual behavior of the small wall during the compression test, the panels were considered simply supported at their bases, pinned at all connections and the top nodes had the displacement constrained in the horizontal direction.

In relation to the geometry adopted, this is in accordance with the average dimensions of the small walls tested in the experimental program. The width and height values are equal to 120.8 cm and 120.20 cm, respectively, with a thickness of 14.06 mm.

Mesh selection and model validation was performed by means of the comparative analysis of the numerical and analytical responses of the compression stress at the base, from the equation that relates the applied load and the contact area. In order to compare the results, an arbitrary load was assumed at the top of the wall. To ensure that the load was evenly distributed on the upper and lower surface of the wall, high rigidity beams were included in the model. Considering the error of 0.05% obtained, the mesh of the masonry macromodel was discretized in 15 elements of 8.0 cm (Fig. 5).

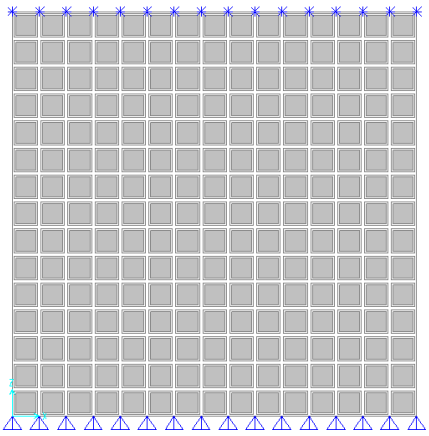

Figure 5 – Discretization of masonry macromodel by SAP2000®

3 Results and discussion

3.1 Numerical, experimental and analytical analysis

In this section experimental, numerical and analytical results are presented and compared Fig. 6 presents the stress-strain experimental curve for five of six walls. The term PP_ALV refers to the small masonry wall. Due to equipment problems in PP_ALV2 the displacement was not measured only being possible to obtain the ultimate strength of this specimen.

The y axis of Fig. 6 shows the compression stress in the small walls, in MPa, and in the x axis the strain for LVDT 1 (in blue) and 2 (in red) are plotted.

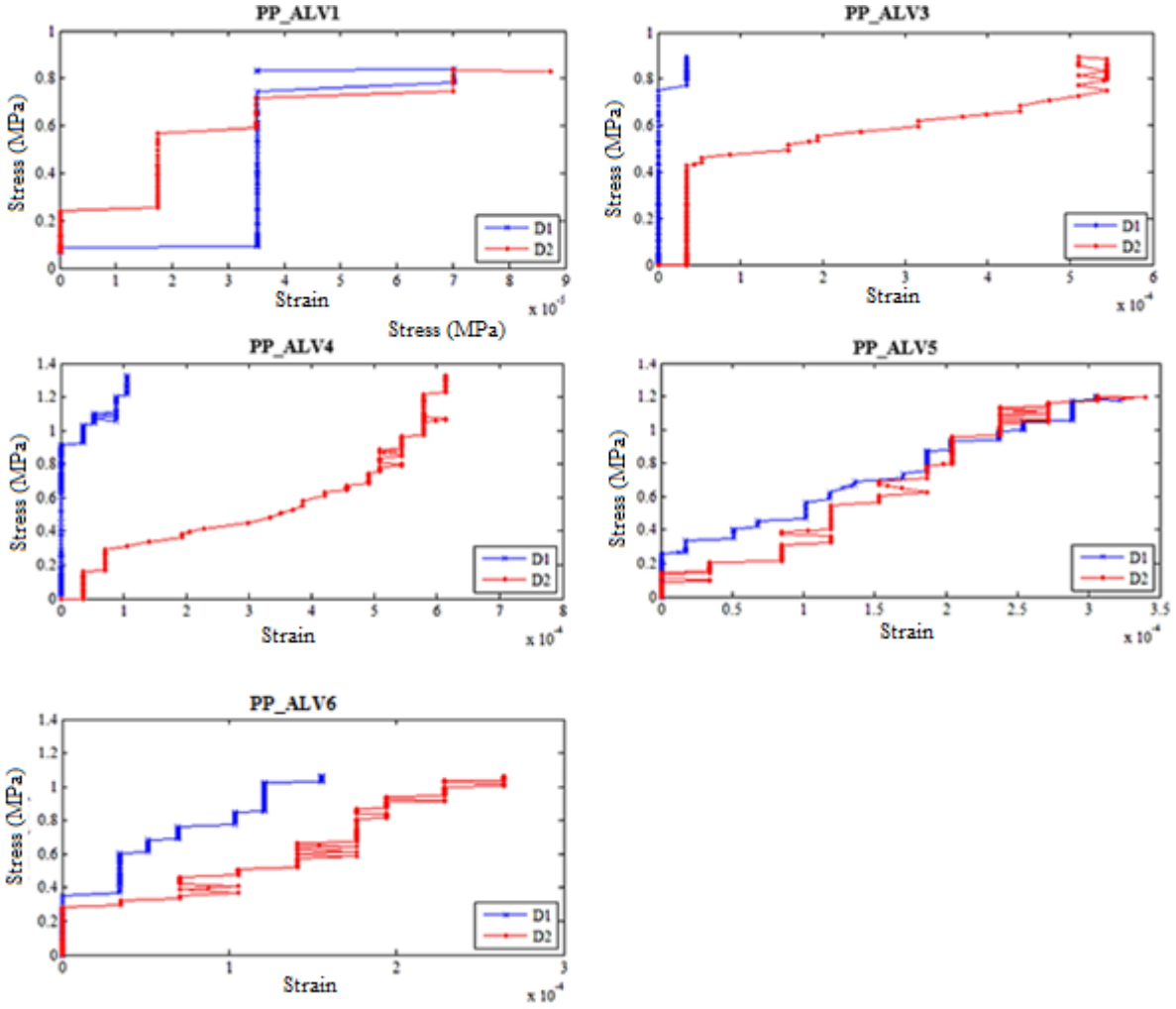

Figure 6. Stress-strain curves experimentally obtained for the small masonry walls

Due the large amount of data collected experimentally, for analytical analysis, ten values of F load were chosen to compare the results. The maximum value of the load considered corresponds to the highest value at which it was possible to obtain strain data in the experimental test. The analytical response was obtained from classical equation $\varepsilon = F/EA$. Where F is the vertical load that is applied on the central studs, the A is the cross-sectional area of the masonry wall and E is the modulus of elasticity in xz plane.

The numerical solution was followed the same methodology, limiting to ten elements the data sample studied. Both analytical and numerical results are presented in Table 4.

In order to facilitate the comparison of the obtained data, Table 4 presents the strains obtained in each analysis for some values of tension. In this table, ε is the strain; subscript D1 and D2 refer to

LVDTs 1 and 2, respectively; and PP_ALV refers to the small masonry wall. In column 4 to 13 are presented the data collected experimentally.

Table 4. Summary of the results obtained in the analytical, numerical and experimental analyzes ($\varepsilon = 10^{-4}$)

Stress (MPa)	ε analytic	ε numerical	PP_ALV1		PP_ALV3		PP_ALV4		PP_ALV5		PP_ALV6	
			ε_{D1}	ε_{D2}	ε_{D1}	ε_{D2}	ε_{D1}	ε_{D2}	ε_{D1}	ε_{D2}	ε_{D1}	ε_{D2}
(1)	(2)	(3)	(4)	(5)	(6)	(7)	(8)	(9)	(10)	(11)	(12)	(13)
0.132	0.42	0.39	0.03	0.00	0.00	0.35	0.00	0.35	0.00	0.00	0.00	0.00
0.264	0.85	0.09	0.35	0.18	0.00	0.35	0.00	0.70	0.12	0.85	0.00	0.00
0.397	1.27	1.31	0.35	0.18	0.00	0.35	0.00	2.05	0.51	1.03	0.35	0.88
0.529	1.69	1.73	0.35	0.18	0.00	1.83	0.00	3.71	1.02	1.19	0.35	1.41
0.661	2.11	2.14	0.35	0.350	0.00	4.39	0.00	4.55	1.33	1.59	0.51	1.41
0.793	2.54	2.56	0,70	0,70	0.35	5.40	0.00	5.43	1.86	1.98	1.04	1.76
0.926	2.96	2.98	-	-	-	-	0.35	5.43	2.03	2.04	1.21	1.94
1.058	3.38	3.40	-	-	-	-	0.53	5.97	2.88	2.72	-	-
1.190	3.81	3.82	-	-	-	-	0.88	5.78	3.05	3.24	-	-
1.322	4.23	4.24	-	-	-	-	1.05	6.13	-	-	-	-

It was verified the convergence between the numerical and analytical values, which presented maximum error of 3.63% % for a tension of 0.132 MPa and almost zero (0.24%) for a tension of 1.322 MPa. The margin of error proves that the choice of the 15x15 mesh generated satisfactory results for the geometric and mechanical parameters adopted in the small walls.

By analyzing data of Table 4, it can be observed that the strain obtained in LVDTs 1 and 2 presented a certain lag between them, without a constant behavior pattern throughout the test (PP_ALV4 e PP_ALV6). The differences are possibly attributed to the lack of plumb observed throughout the experimental test. Another inconsistent behavior was observed for the strain values of PP_ALV1 e PP_ALV3, that kept constant to different tensions. Is this case, the error is possibly related to the period of accommodation of the press during the test. It can be highlighted some another causes that led to small divergences between the numerical and experimental values: i) in the tests, a horizontal displacement of the order 10-4 to 10-3 was verified, however in the numerical model the top nodes were considered plumb; ii) limited LVDT accuracy (± 0.01 mm).

Among the small walls tested, PP_ALV5 presented the most consistent results regarding the measured strains. In the stress range of 0.793 MPa to 1.19 MPa the greatest divergence between the strains obtained in LVDTs 1 and 2 was 5.95%. Table 5 presents some statistical parameters of these numerical and experimental results of PP_ALV5.

Table 5. PP_ALV5 data in a specific range

Stress (MPa)	ε numerical	PP_ALV 5		Mean	Standard deviation (10^{-5})	Absolute error (10^{-5})	Relative error (%)
		$\boldsymbol{\varepsilon_{D1}}$	$\boldsymbol{\varepsilon_{D2}}$				
0.793	2.56	1.86	1.98	1.92	0.833	5.55	27.79
0.926	2.98	2.03	2.04	2.04	0.024	9.23	46.34
1.058	3.40	2.88	2.72	2.80	1.17	5.02	16.72
1.190	3.82	3.05	3.24	3.15	1.36	5.63	16.40

It is observed that the numerical model presented larger strains than those obtained experimentally, suggesting that the modulus of elasticity of the homogenized material is lower than the real one. Even so, for this analyzed range, the maximum absolute error between numerical and experimental response was 0.0000923. Since the values are of the order 10^{-4}, the small variation obtained between the strains generates considerable relative errors.

Table 6 shows the experimental values of the modulus of elasticity for the analyzed range in PP_ALV5, whose average value is 4.06 GPa. New numerical analyzes were then made considering the modulus of elasticity of the macromodel as the experimental average value.

In this case, a significant reduction of the error between numerical and experimental responses was observed.

Table 6. Axial strain of the numerical model with experimental modulus of elasticity

Stress (MPa)	PP_ALV 5 (10^{-4})			Modulus of elasticity (GPa)	ε numerical (10^{-4})	Absolute error (10^{-5})	Relative error (%)
	ε_{D1}	ε_{D2}	ε_{mean}				
0.793	1.86	1.98	1.92	4.13	1.97	-0.35	-1.75
0.926	2.03	2.04	2.04	4.55	2.29	2.55	12.52
1.058	2.88	2.72	2.80	3.78	2.62	-0.67	-2.51
1.19	3.05	3.24	3.15	3.78	2.85	-1.58	-5.26
			Média	4.06			

Regarding the maximum breaking load, considering the small wall resistance 2.54 MPa and the cross-sectional area 0.17 m², the expected theoretical failure load was 431.53 kN. Table 7 presents the data obtained experimentally. For maximum theoretical load of 431.53 kN. The numerical model presented the stress distribution of Fig. 7.

Table 7. Failure modes

	PP_ALV1	PP_ALV2	PP_ALV3	PP_ALV4	PP_ALV5	PP_ALV6	Analytic
Maximum load (kN)	439.7	374.7	394.3	295.6	351.5	333	431.53
Relative error (%)	1.89	-13.17	-8.63	-31.50	-18.55	-22.83	

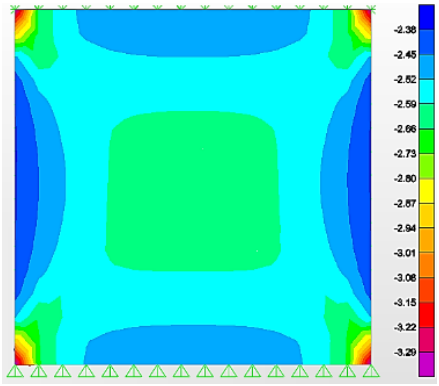

Figure 7. Stress distribution (MPa) in the masonry wall numerical model for theoretical failure load

In Fig. 8 the failure modes of the PP_ALV4 samples. PP_ALV3 and PP_ALV6 are displayed. The rupture occurred near the extremities, confirming the numerically predicted failure region. The other small walls showed an irregular pattern of rupture.

(a) (b) (c)

Figure 8. Failure models of small masonry walls: a) PP_ALV4; b) PP_ALV3 e; c) PP_ALV6

3.2 Comparative analysis of structural efficiency of masonry and light steel frame

To evaluate the structural performance of LSF panels when submitted to compression stress. from an analytical. experimental and numerical approach Nunes et al. [8] developed a study similar to the actual one. The authors analyzed experimentally small walls of LSF with dimensions of 1.20 m x 1.20 m (Fig. 9a) and numerical model (Fig. 9b) were developed in the SAP2000® computer program.

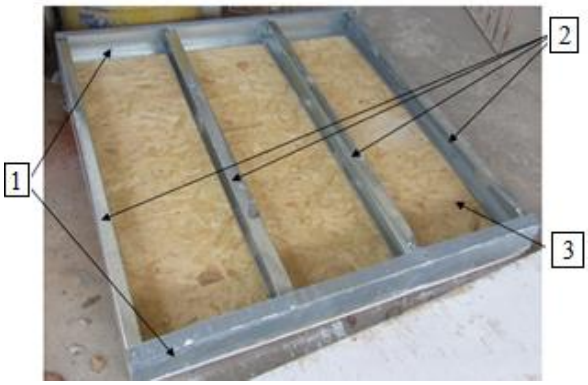

*1. Lip channel tracks; 2. Channels studs; 3. OSB

(a)

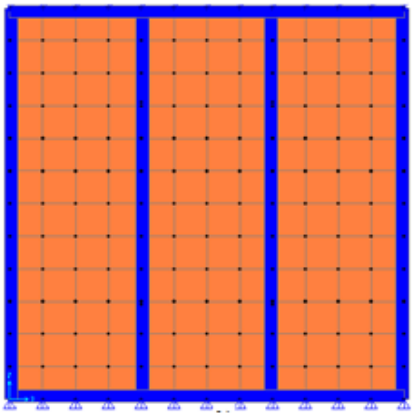

(b)

Figure 9 - Small walls of LSF analyzed (a) experimental e (b) numerically by Nunes et al. [8]

Table 8 presents some results obtained by Nunes et al. [8] to LSF walls. Based on the theoretical and experimental presented values, it can be noted that the structural masonry wall had greater resistance when compared to Light Steel Frame. However. isolated analysis of the maximum load is not sufficient to state that the structural masonry system is more advantageous than the LSF.

Table 8. Summary of the results obtained in the analytical, numerical and experimental analyzes to LSF walls

Stress (MPa)	ε numerical (10^{-4})	PP_LSF1		PP_LSF2		PP_LSF3	
		ε_{D1} (10^{-4})	ε_{D2} (10^{-4})	ε_{D1} (10^{-4})	ε_{D2} (10^{-4})	ε_{D1} (10^{-4})	ε_{D2} (10^{-4})
0.111	0.477	0.00	0.00	-	-	0.00	0.00
0.222	0.949	1.19	2.09	1.12	2.05	0.486	3.32
0.332	1.42	2.53	2.09	2.25	2.41	2.00	5.17
0.443	1.89	3.39	2.41	4.07	3.75	3.24	6.30
0.554	2.36	5.22	2.73	6.42	5.47	4.33	7.28
0.665	2.83	7.29	3.86	8.03	5.79	5.02	8.89
0.776	3.31	10.1	4.18	8.15	5.79	0.557	10.6
0.886	3.78	16.7	4.50	9.38	5.68	0.567	12.6
0.997	4.20	-	-	10.6	7.82	-	-
1.108	4.72	-	-	10.3	9.33	-	-

The average weight of the small structural masonry wall was approximately 270 kg, while the small wall LSF was only 52 kg, which represents less than 20% of the weight of the masonry. From the maximum load / wall weight ratio (Table 9), it can be observed that efficiency of the LSF system is greater than twice that of masonry.

In structural masonry buildings the weight of the walls comprises a significant portion of the vertical loads that must be absorbed by the lower walls themselves. In this case a higher resistance is required to support a higher weight.

Table 9. Efficiency analysis of LSF and masonry walls

Sample	Weight (kg)	Ultimate strength* (kN)	Structural efficiency (kN/kg)
PP_ALV	270	364.8	1.35
PP_LSF	52	144.98	2.79

*Obtained from experimental average values.

According to Gouveia [18], the average weight of a masonry construction is about 1250 kg/m² per floor, considering the occupancy loads. For LSF structures, this value is only 250 kg/m² -, which is 5 times lighter – meaning, so that the metal structure is dimensioned to basically support external loads, and its own influence weight is negligible on the weight of the building.

Concerning the structural safety, as it is a fragile material, the masonry wall ruin occurred suddenly, while in the LSF the strains due to upstream instability gave evidence of the imminent flow of the material.

4 Conclusions

With regard to numerical and analytical analysis, from the obtained results, it can be confirmed that these responses presented an acceptable convergence of values with errors varying between 0.75 and 4.04%. Comparing the numerical and experimental responses, it can be stated that:

i) Analyzing, separately, a stress-strain range value of PP_ALV5, which had more consistent results than the others, it was noted that the mechanical properties of the composite material calculated according to Salamon [6] generated a more deformable model than the real one;
ii) Considering the average value of the modulus of elasticity obtained experimentally, the numerical model presented errors from 1.75 to 12.52%. This rate of change of response is considered satisfactory, given the order of magnitude of the analyzed variable. as well as the limitations of characterization of material properties and the simplifications adopted in the development of the model.
iii) Macromodeling is an efficient tool in the prediction of the mechanisms of transmission of the strength in the masonry.

With regard to comparative analysis of masonry and LSF walls, it was observed that:

iv) Results obtained lead to higher values of resistant load for small walls of structural masonry. However, isolated analysis of this value was considered insufficient, because it does not reproduce the efficiency associated with each system.
v) LSF system was 106.67% more efficient than structural masonry in this study.

References

[1] S. C. Peleteiro, "Contribuições à modelagem numérica de alvenaria estrutural," Escola de Engenharia de São Carlos, Universidade de São Paulo, 2002.
[2] P. B. Lourenc, G. Milani, A. Tralli, and A. Zucchini, "Analysis of masonry structures: review of and recent trends in homogenization techniques," *Can. J. Civ. Eng.*, vol. 34, pp. 1443–1457, 2007.
[3] A. Taliercio, "Closed-form expressions for the macroscopic in-plane elastic and creep coefficients of brick masonry," *Int. J. Solids Struct.*, 2014.
[4] C. Casapulla, A. Maione, L. U. Argiento, and E. Speranza, "Corner failure in masonry buildings: An updated macro-modeling approach with frictional resistances," *Eur. J. Mech. A/Solids*, vol. 70, no. March, pp. 213–225, 2018.
[5] S. Di Nino and A. Luongo, "A simple homogenized orthotropic model for in-plane analysis of regular masonry walls," *Int. J. Solids Struct.*, 2019.

[6] M. D. G. Salamon, "Elastic moduli of a stratified rock mass," *Int. J. Rock Mech. Min. Sci.*, vol. 5, no. 6, pp. 519–527, 1968.

[7] G. N. Pande, J. X. Liang, and J. Middleton, "Equivalent elastic moduli for unit masonry," *Comput. Geotech.*, vol. 8, no. 3, pp. 243–265, 1989.

[8] K. K. F. Nunes, A. C. L. Monteiro, H. J. F. Diógenes, A. B. Silva, and P. V. M. Rezende, "Numerical evaluation to determine the load capacity of light steel frame walls," in *XXXVIII Iberian Latin-American Congress on Computational Methods in Engineering*, 2017.

[9] A. S. P. Barreto, "Análise numérica de painéis de alvenaria estrutural utilizando técnica de homogeneização," Universidade Federal de Pernambuco, 2002.

[10] ASSOCIAÇÃO BRASILEIRA DE NORMAS TÉCNICAS, *ABNT/NBR 12118:2013 - Blocos vazados de concreto simples para alvenaria — Métodos de ensaio.* 2013, p. 14.

[11] ASSOCIAÇÃO BRASILEIRA DE NORMAS TÉCNICAS, *ABNT/NBR 6136:2016 - Blocos vazados de concreto simples para alvenaria — Requisitos.* 2016, p. 1.

[12] ASSOCIAÇÃO BRASILEIRA DE NORMAS TÉCNICAS, *ABNT/NBR 16522:2016 - Alvenaria de blocos de concreto - Métodos de ensaio.* 2016. p. 33.

[13] ASSOCIAÇÃO BRASILEIRA DE NORMAS TÉCNICAS, *ABNT/NBR 13279:2005 - Argamassa para assentamento de paredes e revestimento de paredes e tetos - Determinação da resistência à compressão*. 2005.

[14] ASSOCIAÇÃO BRASILEIRA DE NORMAS TÉCNICAS, *ABNT/NBR 15961-1:2011. Alvenaria estrutural — Blocos de concreto. Parte 1: Projeto.* 2011, p. 42.

[15] ASSOCIAÇÃO BRASILEIRA DE NORMAS TÉCNICAS, *ABNT NBR 15630:2008 Argamassa para assentamento e revestimento de paredes e tetos - Determinação do módulo de elasticidade dinâmico através da propagação de onda ultra-sônica.* 2008, p. 1.

[16] AMERICAN CONCRETE INSTITUTE. *ACI Building Code Requirements for Structural Concrete (ACI 318-11)*. Farmington Hills, MI, 2011.

[17] C. F. R. SANTOS, "Avaliação numérica da interação de paredes de alvenaria estrutural submetidas às ações verticais.," Universidade Federal de Viçosa, 2016.

[18] L. GOUVEIA, "Tudo que ainda não te contaram sobre o Steel Frame: descubra a Verdade aqui.," 2015. [Online]. Available: http://fastcon.com.br/blog/steel-frame/. [Accessed: 29-Jul-2019].